Canadian Journal of Chemistry

OPEN ACCESS | Article

Do we need delocalised wavefunctions for the excited state dynamics of 1,1-difluoroethylene?

Sandra Gómez[a,b], **Nadja K. Singer**[b], **Leticia González**[b], **and Graham A. Worth**[a]

[a]Department of Chemistry, University College London, 20 Gordon Street, London WC1H 0AJ, United Kingdom; [b]Faculty of Chemistry, Institute of Theoretical Chemistry, University of Vienna, Währingerstrasse 17, 1090 Vienna, Austria

Corresponding author: **Sandra Gómez** (email: sandra.gomez@usal.es)

Abstract

In this work, we set up a model Hamiltonian to study the excited state quantum dynamics of 1,1-difluoroethylene, a molecule that has equivalent atoms exchanged by a torsional symmetry operation leading to equivalent minima on the potential energy surface. In systems with many degrees of freedom where the minimum energy geometry is not unique, the ground state wavefunction will be delocalised among multiple minima. In this small test system, we probe the excited state dynamics considering localised (in a single minimum) and delocalised (spread over among multiple minima) wavefunctions and check whether this choice would influence the final outcome of the quantum dynamics calculations. Our molecular Hamiltonian comprises seven electronic states, including valence and Rydberg states, computed with the MS-CASPT2 method and projected onto the vibrational coordinates of the twelve normal modes of 1,1-difluoroethylene in its vibrational ground state. This Hamiltonian has been symmetrised along the torsional degree of freedom to make both minima completely equivalent and the model is supported by the excellent agreement with the experimental absorption spectrum. Quantum dynamics results show that the different initial conditions studied do not appreciably affect the excited state populations or the absorption spectrum when the dynamics is simulated assuming a delta pulse excitation.

Key words: quantum dynamics, excited states, 1,1-difluoroethylene, superpositions

1. Introduction

Symmetry is a powerful tool used to simplify problems and predict properties in a wide range of physical systems. In the context of quantum mechanics applied to molecules, symmetry operations must leave the molecular Hamiltonian invariant, that is, it always belongs to the totally symmetric irreducible representation. For small molecules belonging to non-Abelian symmetry groups, the probability of finding the system in a particular conformation must be exactly the same as finding it in a conformation equivalent by symmetry. The nuclear wavefunction and potential energy surfaces (PES) must then be constructed taking the permutations of the symmetry group into account. The global delocalised wavefunction can be expressed as a superposition of localised wavefunctions at the single minima transformed via symmetry operations. These superpositions have been detected in the laboratory since the Young double slit experiment[1] and much later in buckyballs,[2] and in systems up to 800 atoms.[3] As soon as the system moves away from this relaxed state (i.e., stops being an eigenstate), the expectation values of observables and the wavefunction itself change with time. A question would be whether parts of the superposition might interact differently, maybe due to their relative phase sign, when compared to wavefunctions that are localised in a single minima.

One interesting application where nuclear superpositions are invoked is the theoretical description of nuclear spin isomers (NSIs). The 1920s brought NSIs into the limelight, when the theory about the existence of two different species of the hydrogen molecule (ortho and para) was developed.[4,5] However, even now the separation, identification, and conversion mechanisms between NSIs is a challenging problem and only a few polyatomic molecules (CH_3F,[6–9] $^{13}CH_3F$,[10–12] H_2CO,[13] $^{13}CCH_4$,[14] CH_3OH,[15] H_2O,[16–20] and C_2H_4[21,22]) have been separated in their isomeric forms. In the last 10 years, theories connecting NSIs with superpositions of wavepackets have been developed.[23–31] Using reduced dimensionality models, an association between the nuclear spin and an intermolecular torsion has been made[23,24,27,32–35] and interference of torsional wavepackets within these reduced models leads to different excited state dynamics that can be associated to one or the other NSI, allowing their differentiation.[25,26,36]

Even though the connection between NSIs and rotational levels has been extensively reported, the relation to torsional superpositions (as part of the vibrational wavefunction) has been mostly studied from the theoretical point of view. In this work we will focus on torsional superpositions as initial conditions for the dynamics, without making further connections to NSIs. To the best of our knowledge, every study that has been done using torsional superpositions in the excited

state has used reduced dimensionality models. This is the first time that a full dimensional system is considered, using the case of the 1,1-difluoroethylene (1,1-DFE) molecule in the gas phase, which possesses twelve internal degrees of freedom.

In excited state dynamics, the choice of the initial conditions can critically affect the outcome of a simulation.[37–39] For mixed quantum-classical trajectory methods, such as Tully surface hopping[40] or ab initio multiple spawning,[41] in gas phase simulations geometries and velocities are usually selected from a Wigner distribution that mimics the lowest eigenstate of the ground state quantum harmonic oscillator. In direct dynamics variational multiconfigurational Gaussian (DD-vMCG)[42] methods, a single multi-dimensional Gaussian function that is the solution for the ground state quantum harmonic oscillator carries the initial population. Grid methods like multiconfigurational time dependent Hartree (MCTDH)[43] are very flexible and almost any type of initial wavefunction can be formed and used in the propagation.

For this reason, here dynamics simulations were carried out using the MCTDH method,[44,45] treating explicitly all degrees of freedom at a quantum level. Three different initial conditions were considered: two superpositions, one with a positive relative phase and one negative, and a wavefunction localised in a single minimum, that is, without applying any symmetry operations on it. The deactivation of the population from the valence $\pi\pi^*$ state towards the Rydberg state is found to be not particularly affected by the choice of the initial conditions, that is, superpositions give the same outcome as starting the dynamics in a localised minima. If this behaviour can be extrapolated to larger systems with multiple minima, this result implies an enormous saving in computer time, since only a small part of the configuration space needs to be initially covered.

To describe the full-dimensional PES of 1,1-DFE, we use a vibronic coupling model[46] up to sixth order and fitted to high level ab-initio quantum chemistry calculations at different geometries. Since torsional angles of 90° are needed to arrive at the conical intersections present in this system, the corresponding normal mode needs to be transformed to the actual dihedral angle, and high-order coupling terms (up to the sixth order) need to be included to describe the processes involving this motion with accuracy. In an earlier study on 1,1-DFE using multistate complete active space perturbation theory up to second order (MS-CASPT2) in MOLCAS, we found that a number of Rydberg states must be included to correctly describe the non-adiabatic dynamics starting from the bright valence state.[47]

To prove that our Hamiltonian is indeed a good model, we calculate the absorption spectrum after excitation to the excited-state manifold. The excellent agreement between theoretical and experimental spectrum supports our choice of a Hamiltonian and allows the assignment of the spectral bands. Using a localised initial condition and starting the excited state dynamics from the zwitterionic π^{*2} and Rydberg π-3s, π-3p$_x$, π-3p$_y$, and π-3p$_z$ states, reduced dimensionality models allow us to theoretically unravel the origin of the spectral progression of bands detected in the experimental absorption spectrum of 1,1-DFE.[48]

2. Methods

2.1. Construction of the nuclear Hamiltonian

To analytically describe the PES, we used a vibronic coupling Hamiltonian.[46,49] This method, diabatic by ansatz, expresses the PES as a Taylor expansion around a given point, normally the optimised geometry (Franck-Condon (FC) point). The Hamiltonian $\boldsymbol{H}$ can be thus defined as

$$\boldsymbol{H} = H^{(0)}\mathbf{1} + \boldsymbol{W}^{(0)} + \boldsymbol{W}^{(1)} + \boldsymbol{W}^{(2)} + \boldsymbol{W}^{(3)} + \ldots, \quad (1)$$

where each matrix has a dimension of 7, the number of electronic states involved. As a coordinate basis to express the Hamiltonian, we choose the mass-frequency scaled ground-state normal vibrations, which in the case of 1,1-DFE means 12 normal modes. The zero-order Hamiltonian $H^{(0)}$ corresponds to the kinetic energy operator. For the normal modes q_1–q_3 and q_5–q_{12}, the kinetic energy operator $\widehat{T}_q$ reads

$$\widehat{T}_q = -\sum_{\alpha=1}^{12} \frac{\omega_\alpha}{2} \frac{\partial^2}{\partial Q_\alpha^2}, \quad (2)$$

where ω_α is the ground-state normal mode frequency and α=4 (the torsional degree of freedom) is omitted.

The normal mode q_4 is replaced by the torsion angle θ between the CH_2 group and the molecular plane, considering the fluoride atoms to be fixed due to the large difference in atomic masses. Since a torsional degree of freedom implies a complete rotation along the symmetry axis whereas the normal mode is a harmonic back and forth motion, we transformed the kinetic energy operator following Ref. 50. The kinetic energy operator $\widehat{T}$ for this degree of freedom now reads

$$\widehat{T}_\theta = -\frac{1}{2\mu r^2} \frac{\partial^2}{\partial \theta^2}, \quad (3)$$

where μr^2 corresponds to the moment of inertia with a mass $\mu = 2$ amu, and r is the ground-state equilibrium distance from the hydrogen atoms to the inertial axis (along the CC bond), which is 0.974 Å. The total zero-order Hamiltonian, $H^{(0)}$, is then described as

$$H^{(0)}(Q) = \widehat{T}_\theta + \widehat{T}_q, \quad (4)$$

the sum of both terms.

The matrices **W** form the diabatic potentials and couplings. Following the standard vibronic coupling model scheme, for modes that are close to harmonic (q_1, q_3, q_5, q_7, q_8, q_9, and q_{12}), the zeroth order potential energy matrix $W_{ij}^{(0)}$ is diagonal and formed by the ground-state harmonic oscillator potential shifted by the vertical energies:

$$W_{ij}^{(0)}(Q) = (E_i + V)\,\delta_{ij} = E_i + \sum_\alpha \frac{1}{2}\omega_\alpha Q_\alpha^2; \quad (5)$$
$$\alpha = 1, 3, 5, 7, 8, 9, 12.$$

Higher order terms then enter the appropriate higher order diabatic potential matrices.

Going back to eq. 1, the order of the expansion gives the name for the model: linear vibronic coupling model for expansions truncated at $\boldsymbol{W}^{(1)}$, quadratic vibronic coupling model for truncations at $\boldsymbol{W}^{(2)}$, quartic vibronic coupling model for truncations at $\boldsymbol{W}^{(4)}$, etc. These terms are non-diagonal matrices and are responsible for the coupling, mediated by vibrations, between pairs of electronic states, hence the name of vibronic coupling model. In the 1,1-DFE model, we included expansion terms up to sixth order. The terms up to second order are

$$
\begin{aligned}
(6)\qquad W_{ii}^{(1)}(Q) &= \sum_{\alpha} \kappa_{\alpha}^{(i)} Q_{\alpha} \\
W_{ij}^{(1)}(Q) &= \sum_{\alpha} \lambda_{\alpha}^{(i,j)} Q_{\alpha}\,, \quad i \neq j \\
W_{ii}^{(2)}(Q) &= \sum_{\alpha,\beta} \frac{1}{2} \gamma_{\alpha,\beta}^{(i)} Q_{\alpha} Q_{\beta} \\
W_{ij}^{(2)}(Q) &= \sum_{\alpha,\beta} \frac{1}{2} \mu_{\alpha,\beta}^{(i,j)} Q_{\alpha} Q_{\beta}\,, \quad i \neq j
\end{aligned}
$$

showing how the dependence with the degrees of freedom is linear for the first term, quadratic for the second, etc. Higher-order terms were also required for the diabatic potentials of some modes, in particular for the on-diagonal (intra-state) mode coupling, and are written

$$
\begin{aligned}
(7)\qquad W_{ij}^{(m)}(Q_{\alpha}) &= \frac{1}{m!} C_{\alpha}^{m,(i,j)} Q_{\alpha}^{m} \\
W_{ij}^{(m+n)}(Q) &= \frac{2}{(m+n)!} C_{\alpha,\beta}^{m,n,(i,j)} Q_{\alpha}^{m} Q_{\beta}^{n}.
\end{aligned}
$$

Since 1,1-DFE belongs to the C_{2v} symmetry point group we can apply symmetry to neglect the terms that would make the molecular Hamiltonian antisymmetric. Since the Hamiltonian must be invariant under the symmetry operations of the C_{2v} symmetry point group, some of the Hamiltonian terms are zero by definition. The terms up to second order which are nonzero obey the following product rules for the irreps of the vibrations, Γ_{α}, Γ_{β}, and the irreps of the electronic wavefunctions, Γ_i, Γ_j

$$
\begin{aligned}
(8)\qquad & \kappa_{\alpha}^{(i)} \neq 0: \quad \Gamma_{\alpha} \supset \Gamma_{A_1} \\
& \lambda_{\alpha}^{(i,j)} \neq 0: \ \Gamma_{\alpha} \otimes \Gamma_i \otimes \Gamma_j \supset \Gamma_{A_1} \\
& \gamma_{\alpha,\beta}^{(i)} \neq 0: \ \Gamma_{\alpha} \otimes \Gamma_{\beta} \supset \Gamma_{A_1} \\
& \mu_{\alpha,\beta}^{(i,j)} \neq 0: \Gamma_{\alpha} \otimes \Gamma_{\beta} \otimes \Gamma_i \otimes \Gamma_j \supset \Gamma_{A_1}.
\end{aligned}
$$

This means that the excited state gradients, κ, are only non-zero for totally symmetric modes, while the linear vibronic coupling between states, λ, is due to modes with the correct symmetry that when multiplied by the symmetry of the pair of states leads to a totally symmetric irreducible representation. The diagonal γ terms will be non-zero if the direct product of both modes involved is totally symmetric, whereas for the off-diagonal quadratic coupling terms, μ, the product must also include the symmetry of the electronic states. Symmetry rules for the higher order terms follow as straighforward extensions of these.

Some modes with strong anharmonicity require diabatic potential functions in place of the Taylor expansions described above in order to go to higher orders without drastically increasing the number of parameters to fit. The off-diagonal coupling, however, always follows the scheme above. These anharmonic functions were chosen purely on how well they fitted the ab initio data. Modes q_2 and q_{11} are described by Morse potentials:

$$
(9)\qquad W_{Mor,ii}(Q_{\alpha}) = D_0^{(i)} \left\{ 1 - \exp\left[-a_{\alpha}^{(i)} \left(Q_{\alpha} - Q_{0,\alpha}^{(i)} \right) \right] \right\}^2 + \varepsilon_{\alpha}^{(i)}
$$

and modes q_6 and q_{10} used a Lennard-Jones form

$$
(10)\qquad W_{LJ,ii}(Q_{\alpha}) = -D_0^{(i)} \left[\left(\frac{\left(\alpha_{\alpha}^{(i)}\right)^{12}}{Q_{\alpha} - Q_{0,\alpha}^{(i)}} \right)^{12} - \left(\frac{2\left(\alpha_{\alpha}^{(i)}\right)^{6}}{Q_{\alpha} - Q_{0,\alpha}^{(i)}} \right)^{6} \right] + \varepsilon_{\alpha}^{(i)}.
$$

The torsional q_4 mode, as explained above, is replaced by an angle, θ. Potentials for this mode are periodic and were fitted as a function of the cosine of the torsion angle:

$$
(11)\qquad W_{ii}(\theta) = \kappa_4^{(i)} \cos(\theta) + \frac{1}{2} \gamma_4^{(i)} \cos^2(\theta)\,,
$$

where $\kappa_4^{(i)}$ and $\gamma_4^{(i)}$ are fitting constants. Any diabatic coupling and higher order terms coupling q_4 to the other modes used expressions of the form in eqs. 6 and 7, using $\cos(\theta)$ in place of Q, and taking into account that this function is symmetric at $\theta = 0$ and anti-symmetric at $\theta = \pi$.

The parameters for the functions were obtained using the VCHam tool in the Quantics suite[51] to match the calculated ab-initio data. The 1,1-DFE normal modes were obtained at the planar C_{2v} optimised ground state geometry at the MP2/aug-cc-pVDZ level of theory using the Gaussian 09 program.[52] The normal modes and the corresponding symmetry labels in the C_{2v} point group are depicted in Fig. 1. A comparison between the optimised MP2 geometrical parameters and the experimental values is shown in Table 1. A table with frequencies and description of the motions can be found in the Supporting Information in SI-Table 1.

The electronic state energies of the lowest seven singlet states at torsion angles of 0° and 90° calculated at the SA(11)-MS-CAS(2,6)PT2/aug-cc-pvDZ level of theory are listed in Table 2. The active space includes the Rydberg orbitals 3s, $3p_x$, $3p_y$, and $3p_z$, and the π and π^* orbitals. The state-average procedure is performed over eleven roots to account for every single and double excitation related to the chosen active space (as explained in Ref. 47), even if here we were only interested in the dynamics in the lowest seven states. A picture of the active space and further details about the electronic structure can be found in Ref. 47.

The full dimensional PES consists of twelve nuclear degrees of freedom and 7 electronic states: N, V, Z, π-3s, π-$3p_x$, π-$3p_y$, and π-$3p_z$. N stands for neutral, V for valence and Z for zwitterionic using the Mulliken notation for ethylene.[54] These labels represent the character of the wavefunction at the FC point and are thus used to label the diabatic states of our

Fig. 1. Normal mode coordinate basis with symmetry labels belonging to the C_{2v} point group. The torsional normal mode q_4 is replaced by the full torsion θ in the model Hamiltonian.

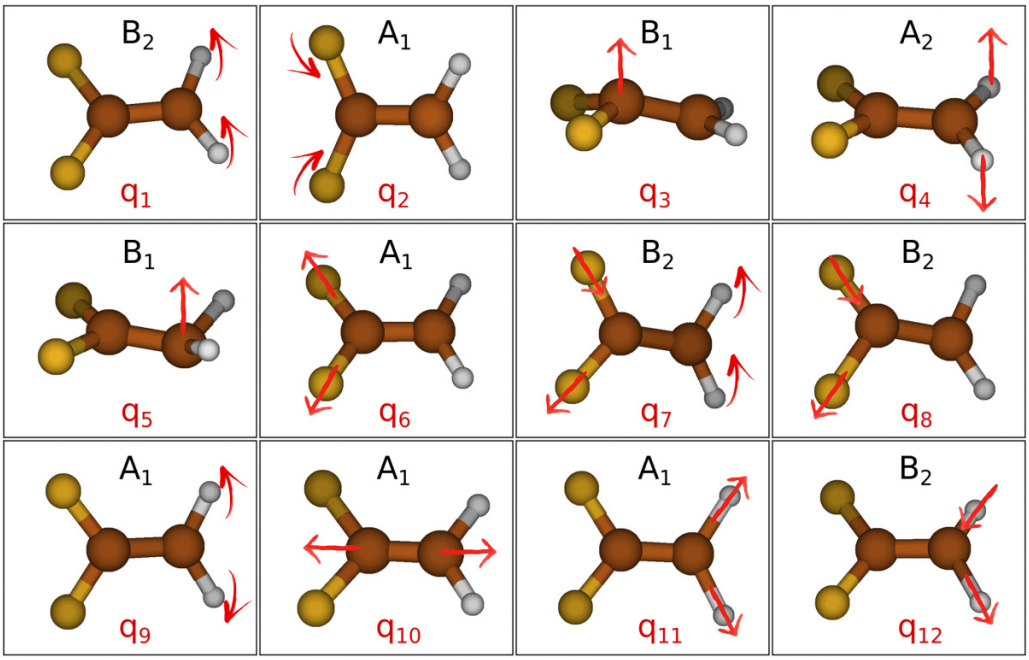

Table 1. Bond lengths (in Ångstrom) and angles (in degrees) for the geometries obtained from the optimisation of the ground state of 1,1-DFE employing MP2/aug-cc-pVDZ in comparison with experimental data from Ref. 53.

	Exp[53]	MP2
r(CC)	1.315	1.335
r(CF)	1.323	1.337
r(CH)	1.078	1.087
∠(FCF)	109.1	109.6
∠(HCH)	121.8	121.5
∠(CCF)	125.5	125.2
∠(HCC)	119.1	119.3

model. Since we need two minima equivalent by torsion to construct the initial wavefunction as a torsional superposition, we transformed our potentials using an orbital diabatic basis. In this basis, the N and V potentials cross and interchange character (see Fig. 2*b*). In this new basis, we rename the states as π_1 and π_2, since they are now completely equivalent. The rest of the states mentioned above keep their original character and thus their labels do not change. The 7 diabatic potential energy curves along the torsion were fitted to ab-initio calculations using the SA(11)-MS-CAS(2,6)PT2/aug-cc-pVDZ level of theory performed at different geometries. Adiabatic curves and single ab-initio points are plotted in Fig. 2*a*. The corresponding diabats are plotted in Fig. 2*b*. The potentials along the original normal mode q_4 can be seen in Fig. 2*c* showing the need of transforming the torsional coordinate in order to describe the crossing to the ground state. The two lowest states cross at 90° of torsion.

To provide data for the fitting, calculations at the FC geometry and at 90° of torsion were performed along every normal mode providing 3234 data points, corresponding to 462 single point electronic structure calculations. The model has 553 parameters to fit which are not independent and so the fitting was done in a series of steps to allow control of the procedure. The diabatic potentials for the torsional degree of freedom were fitted first, using the planar geometry at 0° as the initial point for the Taylor expansion. Next, for every normal mode a 1D fit to the ab-initio data was performed, starting the expansion at 90° of torsion. Explicit couplings to the torsional degree of freedom were then included to force the two minima at planar geometries (0° and 180°) to be equivalent. For every 1D fit, the configuration interaction vector of the electronic structure calculation was monitored, to ensure that the diabats correctly follow their electronic character. For the states π_1 and π_2, however, the same diabatic functions must be used to impose symmetry, which caused some deviations between the ab-initio data and the fitted curves.

After the initial guesses for every diabatic 1D potential were found, a global fit was performed including couplings up to sixth order for specific coordinates (especially couplings that involved the torsional motion). The total standard deviation with respect to the ab-initio points was 0.257 eV, with the largest errors being associated with high energy points that are not well fitted by the model potentials and do not play a role in the dynamics. The 1D adiabatic potential energy curves and the corresponding ab-initio points for three key modes (q_3, q_6, and q_{10}) are plotted in Fig. 3. Cuts along the other degrees of freedom can be found in the Supporting Information. The middle column shows the potential curves at 90° of torsion, where the fit was performed. Note that to

Table 2. Vertical excitations (ΔE, in eV) of 1,1-DFE at the SA(11)-MS-CAS(2,6)PT2/aug-cc-pvDZ level of theory. Three electronic states are labelled following the Mulliken notation for ethylene,[54] N for the closed shell π^2, V for the $\pi\pi^*$ and Z for the π^{*2} state. The energies are calculated at the optimised geometry (FC, for Franck-Condon) and at 90° of torsion. The experimental (exp) values are taken from Ref. 48.

State	ΔE at FC	Exp[48]	Symmetry	ΔE at 90°
N	0.00		A_1	3.30
V	7.45	7.49	A_1	3.47
π-3s	7.07	7.06	B_2	7.91
π-3p_x	8.10		A_2	9.03
π-3p_y	8.20		B_1	9.26
π-3p_z	8.93	8.97	A_1	10.03
Z	13.77		A_1	9.27

Fig. 2. Potential energy curves as a function of the torsional angle θ of 1,1-DFE with all other coordinates at the equilibrium geometry. Fit made using the VCHam tool in the Quantics[51] suite to ab-initio points calculated with SA(11)-MS-CAS(2,6)PT2/aug-cc-pvDZ. (*a*) Adiabatic curves and ab-initio points. (*b*) Diabatic curves. The orbital-diabatic potentials π_1 and π_2 (purple and blue respectively) cross at $\pi/2$ radians and have two equivalent minima at 0 and π radians, each one from a different diabat. (*c*) Ab-initio calculated energy points as a function of the torsional normal mode q_4.

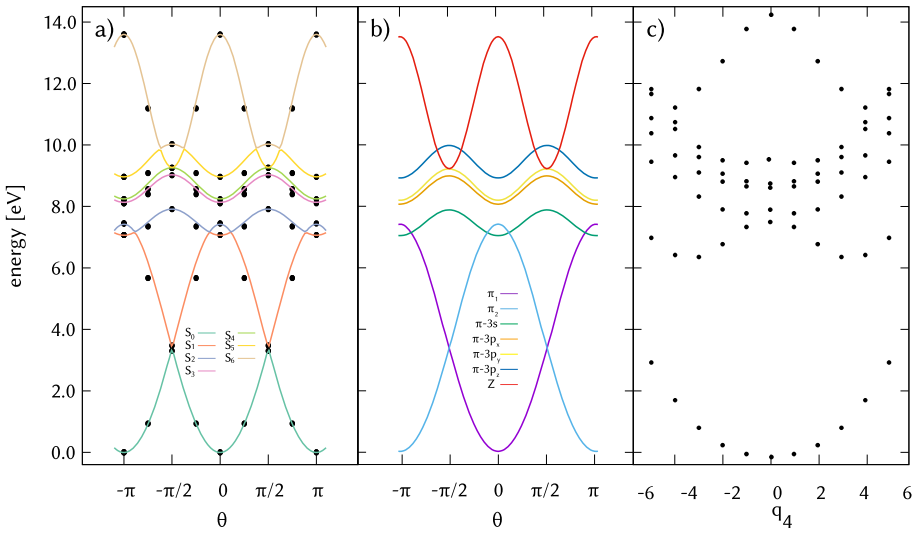

its right and its left, at both 0° and 180° of torsion, the potentials are equivalent, conserving the symmetry. However, these two minima correspond to different diabatic potentials (π_1 and π_2) which switch energetic order at 90°. To preserve the symmetry, these diabatic potentials thus need to be fitted with the same analytical functions and parameters for each normal mode.

All parameters obtained for the model Hamiltonian are listed in the Supporting Information, along with cuts like that in Fig. 3 for all modes showing the quality of the fit.

2.2. Initial conditions

Calculations were performed on different size systems (2D, 5D, and 12D). The initial wavefunction in each calculation was constructed as the Hartree product of the harmonic oscillator ground state for every normal mode and the torsional ground state wavefunction in the π_1 minimum. This was followed by propagation in imaginary time (energy relaxation)[55] to get the ground-state vibrational eigenfunction. The barrier between the minima is high enough that on the timescale of the relaxation (100 fs) there is no transfer of population to the π_2 minimum. Three different initial conditions for the torsional wavefunction were then constructed from this localised wavefunction obtained by relaxation; taken directly as the eigenstate of the π_1, or as positive and negative superpositions to form approximate eigenstates of the π_1 and π_2 diabatic potential energy curves. A scheme can be seen in Fig. 4.

These multidimensional initial wavefunctions created in this way for one or two torsional minima corresponding to states π_1 and π_2 were consequently stored, and read in to be further electronically excited to the π_2 and π_1 states, respectively. This way, either a localised torsional wavefunction or

Fig. 3. Adiabatic potential energy curves along key normal mode coordinates of 1,1-DFE calculated with SA(11)-MS-CAS(2,6)PT2/aug-cc-pvDZ. The right and left columns correspond to torsional angles of π (180°) and 0°, respectively. The middle column corresponds to a torsional angle of $\pi/2$ (90°), where the fit was performed. All other coordinates are at equilibrium values. The labels q_i correspond to the normal mode coordinate along which the ab-initio energies were calculated and fitted. The corresponding normal modes can be seen in Fig. 1.

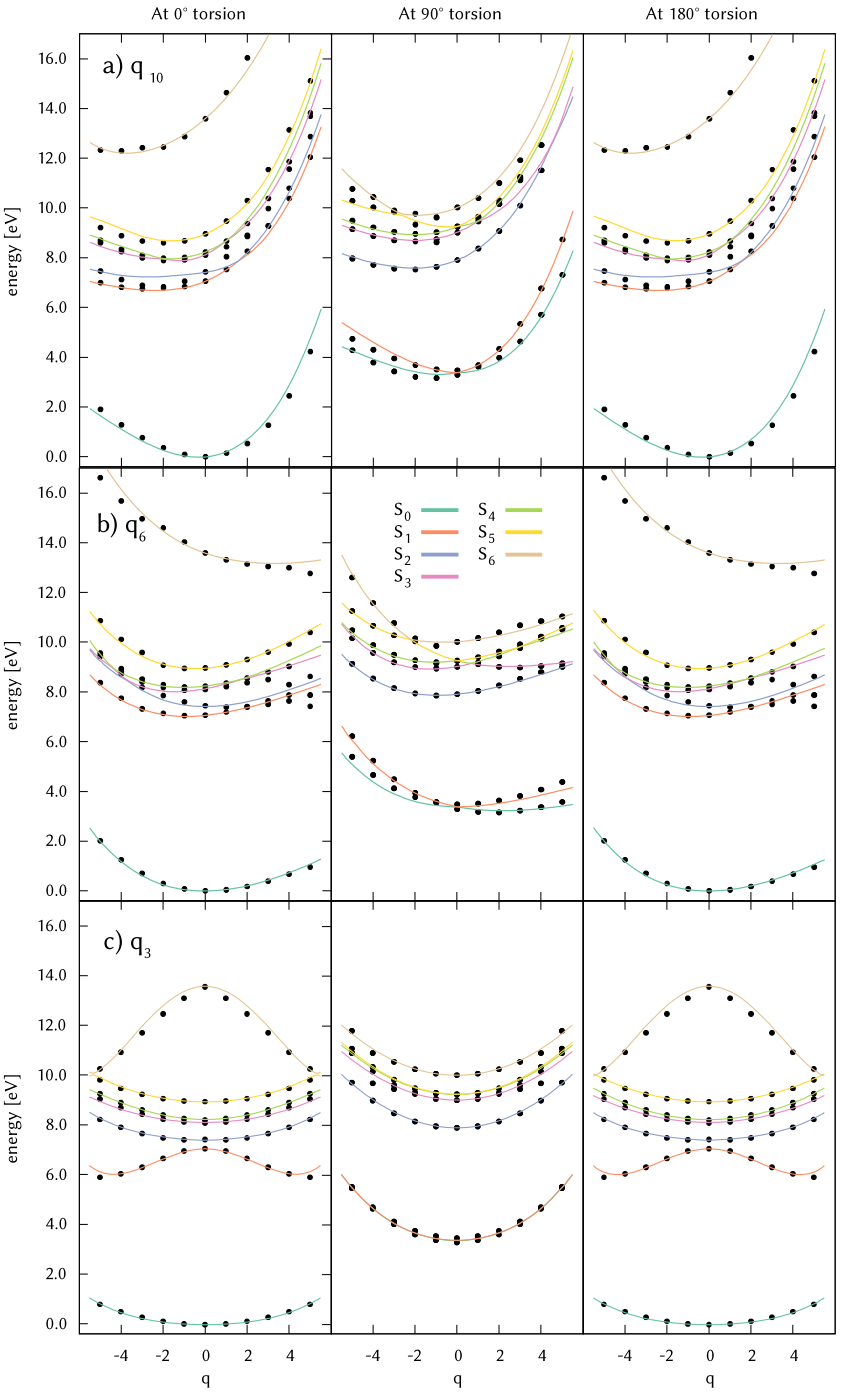

a superposition of them was created in the S_2 adiabatic state (blue state in Fig. 2*a*). In the case of the localised initial condition, the wavefunction carried the whole population, while for the superposition each half was given an amplitude of $1/\sqrt{2}$.

3. Results

3.1. Dynamics started on the $\pi\pi^*$ valence state

Quantum dynamics simulations of 1,1-DFE were performed for symmetric and antisymmetric superpositions as

Fig. 4. Scheme depicting the initial conditions used in this work. Either the symmetric (blue), the antisymmetric (orange), or the localised (just the eigenstate of the left side minima with positive amplitude) were vertically excited to initiate the dynamics.

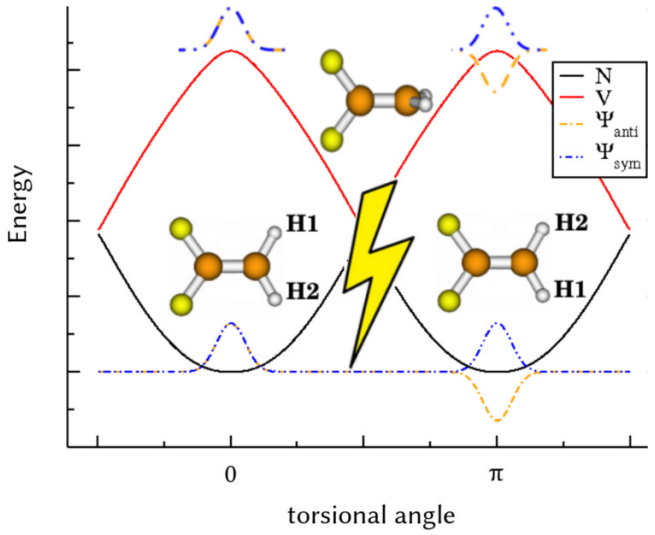

well as for a system localised in one single minima. For each case, a propagation using the MCTDH method was performed for 150 fs, using the multiset formalism, that is, different single particle functions (SPFs) are optimised for each electronic state. The mean fields were calculated at each integration step and integrated with the Adams–Bashforth–Moulton[56] predictor-corrector method. The torsional coordinate was described using a Fast Fourier Transform (FFT) collocation grid, while the other degrees of freedom used harmonic oscillator discrete variable representations (DVRs) as primitive basis functions.

Since convergence of the MCTDH method depends on how the modes are combined within a SPF, on the number of them and on the primitive grid size, we first started converging calculations on a reduced system, to steadily increase the number of degrees of freedom. We performed calculations with two (torsion θ and CC stretching q_{10}), five (torsion θ, CC stretching q_{10}, CF_2 pyramidalization q_3, CF symmetric stretch q_6 and a combination of asymetric CF_2 stretch and CH_2 bend, q_7) and twelve degrees of freedom, that is, full dimensionality (the motions are depicted in Fig. 1). Calculations for the three different initial conditions in all sized systems (2, 5, or twelve degrees of freedom) used the same primitive grids, but were converged individually with respect to the SPF basis. The number of primitive basis functions, along with mode combinations and the number of SPFs per state for the largest calculations performed is found in Table 3.

The dynamics including only two degrees of freedom, q_{10} and θ, shows no interchange of population between the π_1-π_2 states and the π-$3p_x$ state during 150 fs (Fig. 5*a*), indicating that the CC double bond vibration is not enough to drive the system away from the FC region or excite the torsional motion to reach the conical intersections. This agrees with previous work on ethene which showed that for population transfer to occur the pyramidalization motion also needs to be included[59]. The populations of the π_1 and π_2 states have been summed up in the superposition calculations to allow comparison with the localised initial condition that started the dynamics with 100% of its population in π_2. The differences of using or not using a superposition as initial condition are unnoticeable. As we can see in Fig. 5*b*, at least five modes are needed to drive the dynamics, which are qualitatively similar to the full dimensionality result shown in Fig. 5*c*. The population, initially excited to the V state, is very quickly transferred to the π-3s and π-$3p_x$ Rydberg states. This transfer is initially mediated by q_7, a combination of asymmetric CF_2 stretch and CH_2 bend, and the torsional degree of freedom q_4 with the same symmetry as the electronic states and it is driven by the gradient created by the CF symmetric (q_6) and the CC double bond (q_{10}) stretches. In the 5D and 12D cases, the π-$3p_x$ state traps the population during the first 30 fs, after which it slowly relaxes to the π_1-π_2 states and the π-3s. In the 12D case (Fig. 5*c*), the population transferred to the π-3s state is larger than in the reduced dimensionality system, indicating that other degrees of freedom play a role in the excited state dynamics. When comparing the localised and delocalised initial condition 12D runs, we can observe small differences in the populations, probably due to the difficulty of converging the SPF basis in the larger systems.

During the dynamics, the autocorrelation function (overlap of wavefunctions at time=t and time=0) was stored every 0.5 fs and later Fourier transformed to obtain the absorption spectrum. In Fig. 6, the spectrum for the localised initial condition (local) and superpositions with positive (sym) and negative (anti) relative phase are shown for the full system with twelve degrees of freedom. The small differences that can be observed are again probably due to lack of basis set convergence. The main spacing is due to the CC stretching mode (q_{10}) with a harmonic frequency of 0.2192 eV and the shoulder peaks next to the main progression are due to the CF_2 symmetric stretch (q_6, harmonic frequency 0.1132 eV). By comparing to the spectra from reduced dimensionality calculations, the overall width and shape comes from the torsional degree of freedom and the CF symmetric stretches which couple the electronic states, driving the initial wavepacket away from the FC region.

In contrast to a linear vibronic coupling model, our high-order Hamiltonian makes the assignment of which modes couple which states and drive the dynamics impossible after a few femtoseconds. To aid in this task, we performed excited state dynamics based on the 5D propagation shown in Fig. 5*b*, but using only the localised initial condition and removing one degree of freedom each time. The populations and the absorption spectra are depicted in Fig. 7. These simulations show clearly that the torsion and the CF symmetric and CC stretches are crucial to obtain population transfer to any state on the ultrafast timescale, since removing any of these DoFs inhibits the deactivation of the bright state. The CF_2 pyramidalization is needed to allow a transfer to the π-3s state. Although q_7, a combination of asymmetric CF_2 stretch and CH_2 bend, was initially thought to couple the valence and the π-3s state for symmetry reasons, its presence does not affect the outcome of the dynamics. The

Table 3. Basis used for the largest multiconfigurational time dependent Hartree (MCTDH) calculations starting with localised and delocalised (symmetric and antisymmetric) wavefunctions on the $\pi\pi^*$ state. The primitive basis was the harmonic oscillator DVR[57] for every mode except the torsion, which used a periodic Fast Fourier Transform grid.[58] N_i is the number of primitive basis functions for each degree of freedom in the particles, while n_i is the number of single particle functions used for each of the seven electronic states. Config is the total number of configurations in the MCTDH wavefunction.

Type of WF	Particle	N_i	n_i	Config.
2mode				
Local	el	7		7
	θ, q_{10}	100, 55	(1, 1, 1, 1, 1, 1, 1)	
Sym/anti	el	7		7
	θ, q_{10}	100, 55	(1, 1, 1, 1, 1, 1, 1)	
5mode				
Local	el	7		35278
	θ, q_7	100, 27	(10, 29, 26, 8, 3, 3, 4)	
	q_{10}	55	(16, 20, 20, 7, 3, 3, 4)	
	q_3, q_6	31, 27	(10, 30, 20, 10, 3, 3, 4)	
Sym/anti	el	7		54269
	θ, q_7	100, 27	(23, 32, 32, 10, 4, 3, 4)	
	q_{10}	55	(19, 23, 28, 8, 3, 3, 4)	
	q_3, q_6	31, 27	(10, 30, 30, 10, 4, 3, 4)	
12mode				
Local	el	7		229112
	θ, q_{10}	100, 55	(17, 27, 37, 11, 4, 3, 3)	
	q_1, q_2, q_5, q_8	11	(5, 9, 10, 6, 3, 3, 3)	
	q_3, q_6, q_7	31, 27, 27	(17, 29, 30, 9, 4, 3, 4)	
	q_9, q_{11}, q_{12}	11	(10, 11, 12, 6, 4, 3, 3)	
Sym/anti	el	7		619117
	θ, q_{10}	100, 55	(30, 40, 40, 20, 4, 3, 4)	
	q_1, q_2, q_5, q_8	11	(11, 10, 12, 9, 3, 3, 3)	
	q_3, q_6, q_7	31, 27, 27	(30, 40, 40, 20, 4, 3, 4)	
	q_9, q_{11}, q_{12}	11	(13, 13, 13, 9, 4, 3, 3)	

spectra shown in Fig. 7*e* supports the assumption that the torsion dominates the spectrum, since without it we obtain a vibrational progression where the maximum is the 0-0 band. The CF symmetric stretch is responsible for the shoulder peaks and the pyramidalization narrows down the general shape of the spectra when allowing the transfer to the π-3s state.

In our previous work on 1,1-DFE using on-the-fly dynamics,[47] the π-3s state acted as a doorway state, keeping population from the V state trapped for a while before transferring it back. This process was essential for the deactivation of the molecule to its electronic ground state. Using our parametrised potentials and quantum dynamics, we do not see any trapping of the population on this Rydberg state. Instead, its population keeps growing and after 150 fs it is the most populated state. To distinguish between the π_1-π_2 state populations we calculated the adiabatic populations for the 5D localised system integrating the transformed wavefunction over the primitive grids. The electronic ground state population was found to never exceed the value of 0.6%. Therefore, the outcome of the dynamics is substantially different in the two cases and deserves a closer look why this could be.

A quantum dynamics method (like MCTDH) is fully quantum and thus expected to provide a better description of the nuclear motion than that obtained by propagating independent classical trajectories, as done in surface hopping. An important difference in the two calculations is that in surface hopping, the trajectories were selected from a Wigner distribution, which is a quasiprobability function that provides an approximation for the lowest eigenstate of the quantum harmonic oscillator; instead, the MCTDH simulations use the actual lowest energy "localised" eigenfunction of the Hamiltonian for the initial wavefunction. However, to use the MCTDH method, one must pre-compute the PES in advance and fit them to an analytical potential form on a base of nuclear coordinates. This procedure potentially restricts the system as the choice of coordinates and the fitted function may not allow the system to evolve in the same way as with on-the-fly dynamical simulations. As an example, one could think of the different MCTDH dynamics that would result if we had used the torsional normal mode in the model potential and

Fig. 5. Diabatic time-dependent electronic state populations for calculations including (*a*) two nuclear degrees of freedom: torsion and CC stretch, (*b*) five nuclear degrees of freedom: torsion, CC stretch and scissoring, and pyramidalization of CH_2 and CF_2 fragments, and (*c*) twelve degrees of freedom, that is, full dimensionality. In solid lines the population after exciting a localised initial wavefunction (local) is depicted. In dashed and in dotted lines the populations after exciting the symmetric superposition (sym) and the antisymmetric (anti), respectively, are shown.

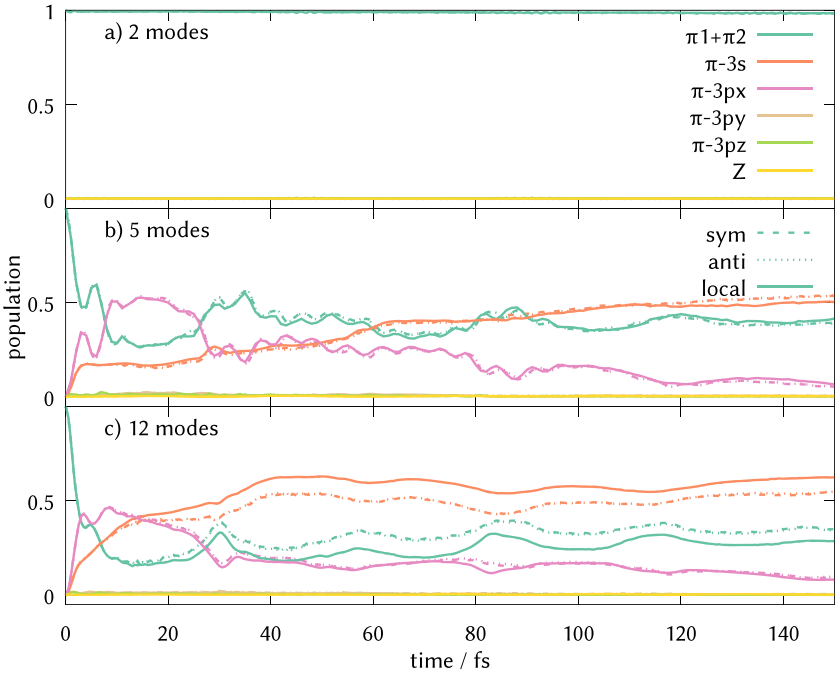

Fig. 6. Absorption spectra calculated as the Fourier transform of the autocorrelation function from full dimensionality dynamics with a damping time (phenomenological broadening) of τ=100 fs comparing an initial condition localised in one minimum (local) a symmetric superposition (sym) and an antisymmetric superposition (anti) started on the V state.

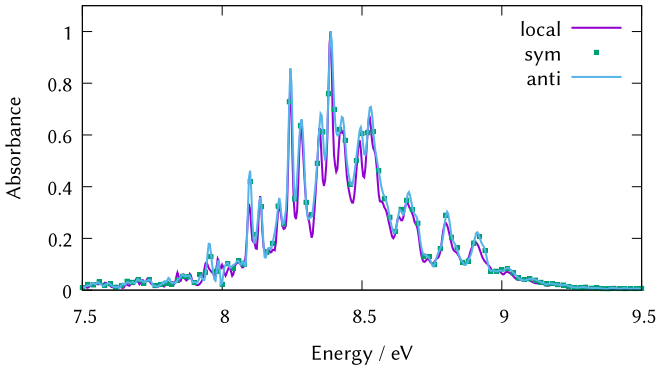

not substituted it by the full dihedral angle, as depicted in Fig. 2. While the quality of the potential used in the MCTDH simulations is supported by the calculated spectrum, the latter only samples the PES around the FC point and does not say anything about the surfaces in general. Furthermore, due to its construction the vibronic coupling model does not include any coupling between modes that requires high-order polynomials.

Further work is thus needed to see which of the two sets of dynamical simulations is correct. A possible protocol would be to run on-the-fly quantum dynamics with the DD-vMCG method,[60,61] but this would require calculating frequencies, gradients, couplings and energies at the CASPT2 level for seven states and each pair of states, which would be computationally very expensive.

3.2. Localised dynamics started on the Rydberg states

In order to extend our excited state dynamics study beyond the the valence $\pi\pi^*$ state, we investigate the dynamics of the system including the manifold of electronic states that couple and affect the behaviour after light irradiation. In Fig. 8*a*, the transition dipole matrix elements that couple the ground state and excited state electronic wavefunctions are plotted at different torsional angles. The values, calculated at the same level of theory as the potentials, refer to the adiabatic electronic states. However, at the ground state optimised geometry the V and π-3s states switch character (see for example Fig. 2) and we accommodated that change switching the values of the matrix elements μ_{12} and μ_{13} at the planar geometry. Since at the FC region the transition dipole moment only has negligible values for the coupling with the π-3p_x state, we started 5D dynamics using the localised initial condition on every other electronic state and calculated the absorption spectra from the autocorrelation function (Fig. 8*b*). Every spectrum has been weighted by the corresponding matrix element of the transition dipole moment

Fig. 7. Simulations corresponding to the five mode dynamics in figure 5 with a localised initial condition, after removing one degree of freedom. (*a*) Diabatic time-dependent populations after removing the torsional θ mode (solid line) and after removing the CF symmetric stretch q_6 (dashed), (*b*) without including the CF_2 pyramidalization q_3, (*c*) ignoring the CC stretch mode q_{10} and (*d*) ignoring q_7, a combination of asymmetric CF_2 stretch and CH_2 bend. (*e*) Absorption spectra computed as the Fourier transform of the autocorrelation function for each of these cases.

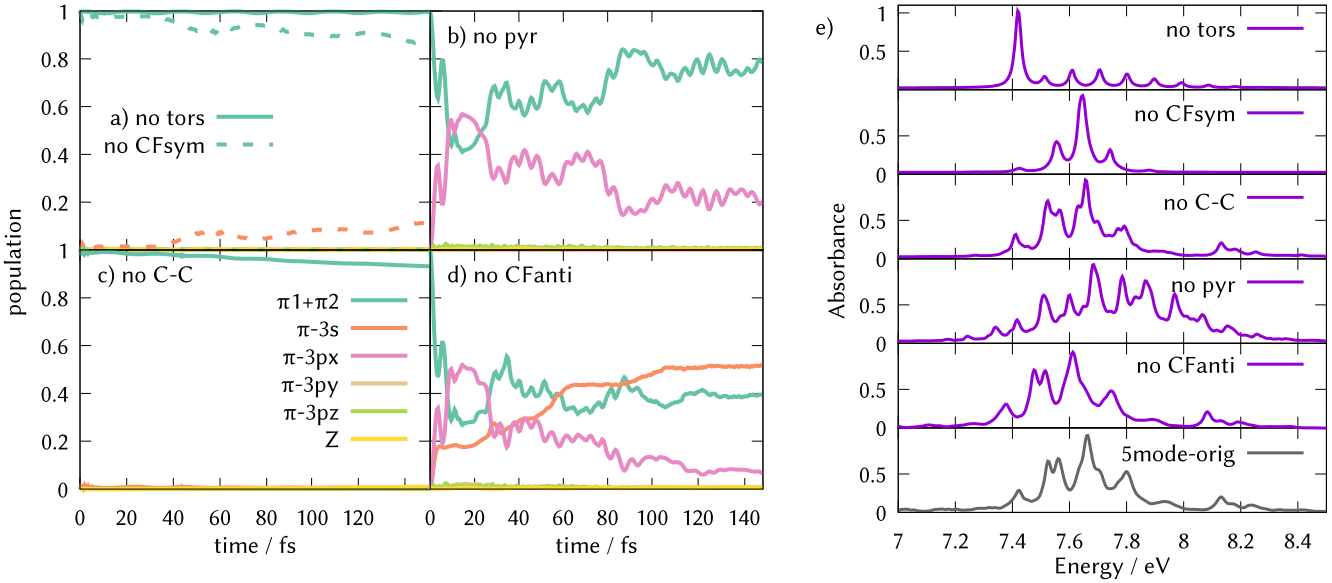

Fig. 8. (*a*) Elements of the adiabatic state transition dipole moment matrix along the torsional degree of freedom calculated with MS-CASPT2. The sub-indices reflect the pair of electronic states involved in the transition. (*b*) Absorption spectra calculated as the Fourier transform of the autocorrelation function from dynamics including five degrees of freedom (except for the V case, where the full dimensionality result was taken), as specified in Table 4 with a damping of $\tau = 50$ fs. Separate calculations were made used a localised initial wavefunction started on the valence, zwitterionic and Rydberg electronic states. The amplitude has been weighted by the transition dipole moments. The experimental spectrum shown in grey was taken from Ref. 48.

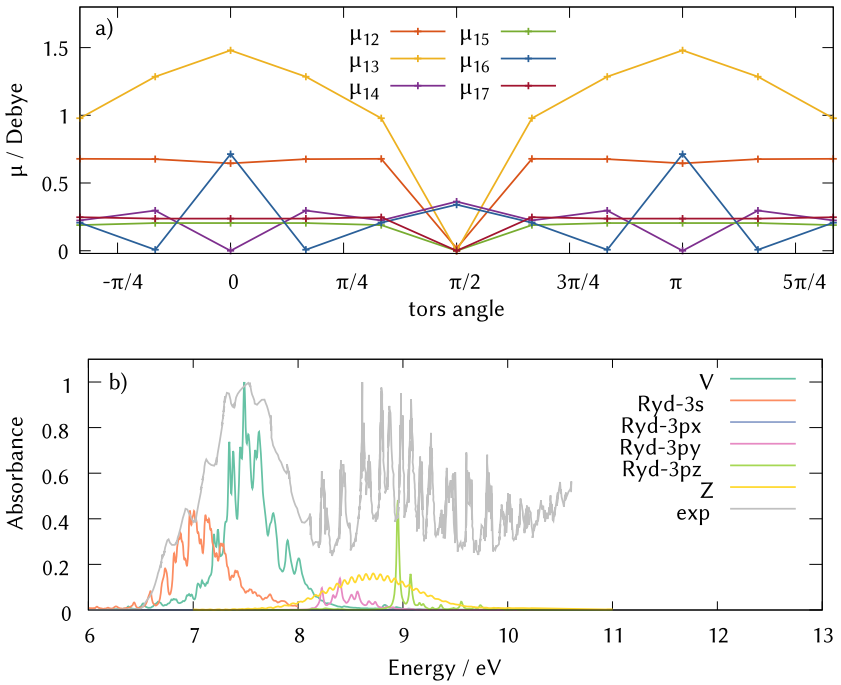

Table 4. Basis used for the multiconfigurational time dependent Hartree (MCTDH) simulations starting with a localised wavepacket on the Rydberg and zwitterionic states. The primitive basis was the harmonic oscillator discrete variable representation for every mode except the torsion, which uses a periodic Fast Fourier Transform grid. N_i is the number of primitive basis per dimension in every particle, while n_i is the number of single particle functions used per electronic state. Config is the total number of configurations in the MCTDH wavefunction.

Initial state	Particle	N_i	n_i	Config.
π-3s	el		7	7130
	θ, q_7	100, 27	(5, 12, 15, 3, 3, 3, 3)	
	q_{10}	55	(10, 14, 12, 4, 4, 3, 3)	
	q_3, q_6	10, 27	(7, 20, 20, 4, 4, 3, 3)	
π-3p$_x$	el		7	46519
	θ, q_7	100, 27	(12, 32, 32, 10, 4, 3, 3)	
	q_{10}	55	(19, 22, 23, 9, 4, 3, 4)	
	q_3, q_6	10, 27	(10, 30, 30, 10, 4, 3, 4)	
π-3p$_y$	el		7	45105
	θ, q_7	100, 27	(9, 32, 31, 10, 4, 3, 4)	
	q_{10}	55	(16, 22, 23, 10, 4, 3, 4)	
	q_3, q_6	10, 27	(10, 30, 30, 10, 4, 3, 4)	
π-3p$_z$	el		7	26490
	θ, q_7	100, 27	(7, 13, 28, 10, 4, 4, 3)	
	q_{10}	55	(11, 19, 25, 10, 4, 3, 4)	
	q_3, q_6	10, 27	(10, 23, 27, 10, 4, 3, 4)	
Z	el		7	68355
	θ, q_7	100, 27	(24, 32, 32, 10, 4, 3, 4)	
	q_{10}	55	(24, 32, 32, 10, 4, 3, 4)	
	q_3, q_6	10, 27	(10, 30, 30, 10, 4, 3, 4)	

at the FC point. The spectrum starting in the V state has been computed from dynamics in full dimensionality (it is the same as Fig. 6) and therefore has been shifted in energy by the difference in the zero point energies due to the extra degrees of freedom. In Ref. 48, the first band is concluded to be a mixture of the Rydberg π-3s and the valence $\pi\pi^*$ states. The vibrational progression observed at higher energies starts with peaks from the π-3p$_y$ state, followed by the π-3p$_z$ and probably higher lying Rydberg states. The Z state modulates the intensity of these peaks with a broad gaussian-like shape.

4. Conclusions

We set out to investigate the importance of superpositions due to symmetrically equivalent minima to describe the initial wavepacket in photo-excited quantum dynamics simulations. The answer is found to be in the negative and no significant difference was seen in the excited state quantum dynamics of the 1,1-DFE molecular system using either localised (single minimum) or delocalised (symmetry-adapted) initial conditions. We observe that a qualitative correct behaviour of the deactivation of the V state is achieved with five degrees of freedom from the total of twelve. The torsion, CC and CF symmetric stretches, combination of asymmetric CF_2 stretch and CH_2 bend, and the CF_2 pyramidalization drive the excited state dynamics on this system and explain the peaks observed in the absorption spectra after Fourier transforming the autocorrelation function.

In contrast to previous Tully surface hopping dynamics,[47] the current simulations find that there is barely population transfer to the electronic ground state, flowing into the Rydberg π-3s instead. This outcome is consistent for all three initial conditions investigated, illustrating that using a localised nuclear wavefunction is perfectly reasonable and the relative phases on the parts of the symmetric and antisymmetric superpositions do not affect the dynamics, leading to numerically identical results. There are minor differences for the full-dimensional system when starting with a localised wavefunction which is maybe due to convergence. As a way of validating our parameterised Hamiltonian, we performed dynamics using a localised initial condition on the valence, zwitterionic, and Rydberg electronic states and calculated absorption spectra weighted by the oscillator strengths that couple those states with the electronic ground state. An excellent agreement with the experimental spectrum measured in Ref. 48 supports our model.

Acknowledgements

We thank the MOLecules In Motion COST Action (CM1405) for funding short term scientific missions from the University of Vienna to University College London that made this collaboration possible. SG acknowledges NextGenerationEU

funds (María Zambrano Grant for the attraction of international talent). GW thanks the EPSRC for funding through grant EP/S028781/1.

Article information

History dates

Received: 13 October 2022
Accepted: 10 February 2023
Accepted manuscript online: 6 April 2023
Version of record online: 31 May 2023

Notes

This paper is one of a selection of papers from the 12th Triennial Congress of the World Association of Theoretical and Computational Chemists (WATOC 2020).

Copyright

Data availability

Extra information such as ground state normal mode frequencies, potential energy curves along the twelve degrees of freedom and ab initio points against which the curves are fitted, parameters for the one-dimensional diabatic potentials and intra-state, linear, and bilinear coupling parameters can be found in the Supporting Information. The quantics inputs and operator file are deposited at the UCL Repository https://rdr.ucl.ac.uk. DOI: 10.5522/04/21318339.

Author information

Author ORCIDs

Sandra Gómez https://orcid.org/0000-0002-1874-6578
Graham A. Worth https://orcid.org/0000-0002-2044-4499

Author notes

Present address for Sandra Gómez is Departamento de Química Física, University of Salamanca, 37008, Spain.

Authors contribution statement

Conceptualization: LG
Formal analysis: SG, NKS
Funding acquisition: LG
Investigation: SG, NKS
Methodology: SG
Project administration: LG
Resources: LG
Software: SG, GAW
Supervision: LG, GAW
Validation: SG, NKS, GAW
Visualization: SG
Writing – original draft: SG, GAW
Writing – review & editing: SG, NKS, LG, GAW

Competing interests

There are no competing interests to declare.

Supplementary material

Supplementary data are available with the article at https://doi.org/10.1139/cjc-2022-0267.

References

1. Young, T. Phil. Trans. R. Soc. Lond., **1802**, *92* 12–48.
2. Arndt, M., Nairz, O., Vos-Andreae, J., Keller, C., van der Zouw, G., Zeilinger, A. Nature, **1999**, *401*, 680. doi:10.1038/44348.
3. Eibenberger, S., Gerlich, S., Arndt, M., Mayor, M., Tüxen, J. Phys. Chem. Chem. Phys., **2013**, *15* **14696**.
4. Hund, F. Z. Phys., **1927**, *42*, 93. doi:10.1007/BF01397124.
5. Heisenberg, W. Z. Phys., **1927**, *41* 239. doi:10.1007/BF01391241.
6. Panfilov, V. N., Strunin, V. P., Chapovsky, P. L. Sov. Phys. J. Exp. Theor. Phys., **1983**, *58*, 510.
7. Chapovsky, P. L., Krasnoperov, L. N., Panfilov, V. N., Strunin, V. P. Chem. Phys., **1985**, *97*, 449. doi:10.1016/0301-0104(85)87052-X.
8. Bakarev, A. E., Chapovsky, P. L. J. Exp. Theor. Phys. Lett., **1986**, *44*, 4.
9. Chapovsky, P. L. Sov. Phys. J. Exp. Theor. Phys., **1990**, *70*, 895.
10. Nagels, B., Schuurman, M., Chapovsky, P. L., Hermans, L. J. F. Phys. Rev. A, **1996**, *54* 2050. doi:10.1103/PhysRevA.54.2050.
11. Nagels, B., Hermans, L. J. F., Chapovsky, P. L. Phys. Rev. Lett., **1997**, *79*, 3097. doi:10.1103/PhysRevLett.79.3097.
12. Cacciani, P., Coslóu, J., Herlemont, F. Khelkhal, M., Lecointre, J. Phys. Rev. A, **2004**, *69*, 1. doi:10.1103/PhysRevA.69.032704.
13. Peters, G., Schramm, B. Chem. Phys. Lett., **1999**, *302* 181. doi:10.1016/S0009-2614(99)00042-1.
14. Chapovsky, P. L., Cosléou, J., Herlemont, F., Khelkhal, M., Legrand, J. Chem. Phys. Lett., **2000**, *322*, 424. doi:10.1016/S0009-2614(00)00445-0.
15. Ge Zhen-Dong Sun, M., Zheng, Y. Nat. Commun., **2015**, *6*, 6877. doi:10.1038/ncomms7877.
16. Konyukhov, V. K., Prokhorov, A. M., Tikhonov, V. I., Faizulaev, V. N. J. Exp. Theor. Phys., **1986**, *43*, 65.
17. Tikhonov, V. I., Volkov, A. A. Science, **2002**, *296* 2363. doi:10.1126/science.1069513.
18. Kravchuk, T., Reznikov, M., Tichonov, P., Avidor, N., Meir, Y., Bekkerman, A., Alexandrowicz, G. Science, **2011**, *331*, 319. doi:10.1126/science.1200433.
19. Horke, D. A., Chang, Y.-P., Dlugolecki, K., Küpper, J. Angew. Chem. Int. Ed., **2014**, *53* 11965. doi:10.1002/anie.201405986.
20. Kilaj, A., Gao, H., Rösch, D., Rivero, U., Küpper, J., Willitsch, S. Nat. Commun., **2018**, *9*, 2096. doi:10.1038/s41467-018-04483-3.
21. Sun, Z.-D., Takagi, K., Matsushima, F. Science, **1938**, *310*, 2005.
22. Zhivonitko, V. V., Kovtunov, K. V., Chapovsky, P. L., Koptyug, I. V. Angew. Chem. Int. Ed., **2013**, *52*, 13251. doi:10.1002/anie.201307389.
23. Grohmann, T., Leibscher, M. J. Chem. Phys., **2011**, *134*, 204316. doi:10.1063/1.3595133.
24. Floß, J., Grohmann, T., Leibscher, M., Seideman, T. J. Chem. Phys., **2012**, *136*, 084309. doi:10.1063/1.3687343.
25. Obaid, R., Kinzel, D., Oppel, M., González, L. J. Chem. Phys., **2014**, *141*, 164323. doi:10.1063/1.4899178.
26. Obaid, R., Kinzel, D., Oppel, M., González, L. Theor. Chem. Acc., **2015**, *134*, 46. doi:10.1007/s00214-015-1644-4.
27. Belz, S., Deeb, O., González, L., Grohman, T., Kinzel, D., Leibscher, M., Manz, J., Obaid, R., Oppel, M., Xavier, G. D., Zilberg, S. Z. Phys. Chem., **2013**, *227*, 1021. doi:10.1524/zpch.2013.0385.
28. Grohmann, T., Haase, D., Jia, D., Manz, J., Yang, Y. J. Chem. Phys., **2018**, *149*, 184302. doi:10.1063/1.5048358.
29. Jia, D., Manz, J., Yang, Y. AIP Adv., **2018**, *8*, 045222. doi:10.1063/1.5028573.
30. Lu, X.-Q., Man, Y., Ruß, V., Xu, Y., Yang, Y., Li, S.-D. Phys. Chem. Chem. Phys., **2021**, *23*, 19146–19149. doi:10.1039/D1CP02980K.
31. Yang, H., Man, Y., Wang, H., Yang, Y. Chem. Phys., **2022**, *562*, 111659. doi:10.1016/j.chemphys.2022.111659.

32. Gómez, S., Oppel, M., González, L. Chem. Phys. Lett., **2017**, *683*, 205. doi:10.1016/j.cplett.2017.03.022.
33. Deeb, O., Leibscher, M., Manz, J., von Muellern, W., Seideman, T. Chem. Phys. Chem., **2007**, *8*, 322. doi:10.1002/cphc.200600543.
34. Grohmann, T., Deeb, O., Leibscher, M. Chem. Phys., **2007**, *338*, 252. doi:10.1016/j.chemphys.2007.05.020.
35. Belz, S., Grohmann, T., Leibscher, M. J. Chem. Phys., **2009**, *131*, 034305. doi:10.1063/1.3175800.
36. Waldl, M., Oppel, M., González, L. J. Phys. Chem. A, **2016**, *120*, 4907. doi:10.1021/acs.jpca.5b12542.
37. Barbatti, M., Sen, K. Int. J. Quant. Chem., **2016**, *116*, 762–771. doi:10.1002/qua.25049.
38. Suchan, J., Hollas, D., Curchod, B. F. E., Slavíček, P. Faraday Discuss., **2018**, *212*, 307–330. doi:10.1039/C8FD00088C.
39. Avagliano, D., Lorini, E., González, L. Phil. Trans. R. Soc., A, **2022**, *380*, 20200381. doi:10.1098/rsta.2020.0381.
40. Tully, J. C., Preston, R. K. J. Chem. Phys., **1971**, *55*, 562. doi:10.1063/1.1675788.
41. Ben-Nun, M., Martínez, T. J. Ab Initio Quantum Molecular Dynamics. John Wiley and Sons, **2002**.
42. Richings, G. W., Polyak, I., Spinlove, K. E., Worth, G. A., Burghardt, I., Lasorne, B. Int. Rev. Phys. Chem., **2015**, *34*, 269. doi:10.1080/0144235X.2015.1051354.
43. Beck, M. H., Meyer, H.-D. Z. Phys. D. Atom. Mol. Cl., **1997**, *42*, 113. doi:10.1007/s004600050342.
44. Beck, M. H., Jäckle, A., Worth, G. A., Meyer, H.-D. Phys. Rep., **2000**, *324*, 1. doi:10.1016/S0370-1573(99)00047-2.
45. Meyer, W. G. A.-D., Köppel, H., Cederbaum, L. S., Burghardt, I. Int. Rev. Phys. Chem., **2008**, *27*, 569–606. doi:10.1080/01442350802137656.
46. Köppel, H., Domcke, W., Cederbaum, L. S. Adv. Chem. Phys., **1984**, *57*, 59.
47. Gómez, S., Ibele, L. M., González, L. Phys. Chem. Chem. Phys., **2019**, *21*, 4871. doi:10.1039/C8CP07766E.
48. Vieira, P. L., Vasekova, E., Sekhar, B. N. R., Mason, N. J., Hoffman, S. V. Phys. Chem. Chem. Phys., **2006**, *8*, 4766. doi:10.1039/B610978K.
49. Worth, G. A., Cederbaum, L. S. Ann. Rev. Phys. Chem., **2004**, *55*, 127–158. doi:10.1146/annurev.physchem.55.091602.094335.
50. Cattarius, C., Worth, G. A., Meyer, H.-D., Cederbaum, L. S. J. Chem. Phys., **2001**, *115*, 2088–2100. doi:10.1063/1.1384872.
51. Worth, G. A., Giri, K., Richings, G. W., Beck, M. H., Jäckle, A., Meyer, H.-D. QUANTICS, a suite of programs for molecular QUANTum dynamICS simulations, Version 1.1, **2015**.
52. Frisch, M. J., Trucks, G. W., Schlegel, H. B., Scuseria, G. E., Robb, M. A., Cheeseman, J. R., Scalmani, G., Barone, V., Mennucci, B., Petersson, G. A., Nakatsuji, H., Caricato, M., Li, X., Hratchian, H. P., Izmaylov, A. F., Bloino, J., Zheng, G., Sonnenberg, J. L., Hada, M., Ehara, M., Toyota, K., Fukuda, R., Hasegawa, J., Ishida, M., Nakajima, T., Honda, Y., Kitao, O., Nakai, H., Vreven, T., Montgomery, J. A., Jr., Peralta, J. E., Ogliaro, F., Bearpark, M., Heyd, J. J., Brothers, E., Kudin, K. N., Staroverov, V. N., Kobayashi, R., Normand, J., Raghavachari, K., Rendell, A., Burant, J. C., Iyengar, S. S., Tomasi, J., Cossi, M., Rega, N., Millam, J. M., Klene, M., Knox, J. E., Cross, J. B., Bakken, V., Adamo, C., Jaramillo, J., Gomperts, R., Stratmann, R. E., Yazyev, O., Austin, A. J., Cammi, R., Pomelli, C., Ochterski, J. W., Martin, R. L., Morokuma, K., Zakrzewski, V. G., Voth, G. A., Salvador, P., Dannenberg, J. J., Dapprich, S., Daniels, A. D., Farkas Foresman, J. B., Ortiz, J. V., Cioslowski, J., Fox, D. J. Gaussian 09 Revision A.1. Gaussian Inc. Wallingford CT **2009**.
53. Kovner, M. A., Sverdlov, L. M., Krainov, E. P. J. Mol. Struct., **1975**, *26*, 136.
54. Mulliken, R. S. Phys. Rev., **1933**, *43*, 279. doi:10.1103/PhysRev.43.279.
55. Auer, J., Krotscheck, E., Chin, S. A. J. Chem. Phys., **2001**, *115*, 6841. doi:10.1063/1.1404142.
56. Burden, R. L., Faires, J. D. Numerical Analysis. Boston PWS-Kent Pub. Co, 5th edition, **1993**.
57. Light, J. C., Hamilton, I. P., Lill, J. V. J. Chem. Phys., **1985**, *82*, 1400. doi:10.1063/1.448462.
58. Kosloff, D., Kosloff, R. J. Comput. Phys., **1983**, *52*, 35. doi:10.1016/0021-9991(83)90015-3.
59. Ben-Nun, M., Martínez, T. J. Chem. Phys., **2000**, *259*, 237. doi:10.1016/S0301-0104(00)00194-4.
60. Christopoulou, G., Freibert, A., Worth, G. A. J. Chem. Phys., **2021**, *154*, 124–127.
61. Richings, G. W., Worth, G. A. Chem. Phys. Lett., **2017**, *683*, 606–612. doi:10.1016/j.cplett.2017.03.032.